

## N91-27634

2

## IMPROVED REFERENCE MODELS FOR MIDDLE ATMOSPHERE OZONE

G. M. Keating<sup>1</sup>, M. C. Pitts<sup>2</sup>, and C. Chen<sup>2</sup><sup>1</sup>Atmospheric Sciences Division, NASA Langley Research Center, Hampton, VA 23665<sup>2</sup>ST Systems Corporation (STX), Hampton, VA 23666

## ABSTRACT

Improvements are provided here for the ozone reference model which is to be incorporated in the COSPAR International Reference Atmosphere (CIRA). The ozone reference model will provide considerable information on the global ozone distribution, including ozone vertical structure as a function of month and latitude from approximately 25 to 90 km, combining data from five recent satellite experiments (Nimbus 7 LIMS, Nimbus 7 SBUV, AE-2 SAGE, Solar Mesosphere Explorer (SME) UVS, and SME IR). The improved models described here use reprocessed AE-2 SAGE data (sunset) and extend the use of SAGE data from 1981 to the period 1981-1983. It is found that these SAGE data agree at all latitudes and months with the ozone reference model within 15 percent and result in modifications in the reference model of less than 4 percent. In the mesosphere, a model of nighttime conditions (= 10 p.m.) has been added using Nimbus 7 LIMS data between pressures of 0.5 mb to 0.05 mb (= 54 to 70 km). Minimum nighttime ozone mixing ratios occur at about 0.2 mb (= 61 km). The ratio of nighttime LIMS data to daytime (= 3 p.m.) SME data gives diurnal variations as large as a factor of 6 at the highest levels. At 0.1 mb (= 66 km), the night-day diurnal variation can exceed 3 and maximizes during solstice periods near 45 degrees in the summer hemisphere and near the Equator during equinoctial periods. This may largely result from the daytime ozone being more strongly photodissociated by the more directly incident summer Sun at mid latitudes and the equinoctial Sun at the Equator. Comparisons are shown between the ozone reference model and various non-satellite measurements at different levels in the middle atmosphere.

## INTRODUCTION

An ozone reference model is being developed for incorporation in the next COSPAR International Reference Atmosphere (CIRA). Previous versions of the Keating et al. model are described in the ozone chapter in the "Draft Reference Middle Atmosphere" published in Map Handbook Number 16 /1/ and in editions of Advances in Space Research /2, 3, 4/. The ozone vertical structure from = 25 to 90 km is determined by combining results from five contemporary satellite experiments: Nimbus 7 Solar Backscatter Ultraviolet (SBUV), Applications Explorer Mission-2 Stratospheric Aerosol Gas Experiment (SAGE), Solar Mesosphere Explorer (SME) UV Spectrometer (SME-UVS), and SME 1.27 Micron Airglow (SME-IR). Total column ozone is determined using Nimbus 7 TOMS data. Monthly standard deviations in the zonal mean ozone are provided for both the vertical structure and total column ozone, indicators of the interannual variability are given, and models developed by /5/ relating vertical structure of ozone to total column ozone for low, medium, and high latitudes are also included in the Keating and Young representation. A brief discussion is also provided by Keating and Young /1/ of the various systematic variations in ozone which have been studied, including the annual and semiannual variations and quasi-biennial oscillation, estimates of solar rotation and solar-cycle variations, diurnal variations, longitudinal variations, possible variations with volcanic eruptions and nuclear explosions, response to solar proton events, response to stratospheric temperature variations, possible 4-year oscillations, and long-term trends.

In this paper, the models of vertical structure are improved using reprocessed AE-2 SAGE data as one of the data sets for the period 1981-1983. Previously, only SAGE data from 1981 had been used. Also, models of the nighttime mesospheric ozone are provided using Nimbus 7 LIMS data from 0.5 mb to 0.05 mb (= 54 to 70 km). The reference model is compared with various non-satellite measurements of ozone.

The pressure range and time intervals of the data used in these improved models are shown in Table 1.

TABLE 1 Satellite Data Used for Improved Ozone Reference Models

Instrument	Incorporated Pressure Range	Incorporated Time Interval
Nimbus 7 LIMS	0.5 - 20 mb 0.05 - 0.5 mb (night)	11/78 - 5/79 11/78 - 5/79
Nimbus 7 SBUV	0.5 - 20 mb	11/78 - 9/82
AE-2 SAGE	5 - 20 mb	2/79 - 11/81
SME UVS	0.07 - 0.5 mb	1/82 - 12/83
SME IR	0.003 - 0.5 mb	1/82 - 12/83
Nimbus 7 TOMS	TOTAL	11/78 - 9/82

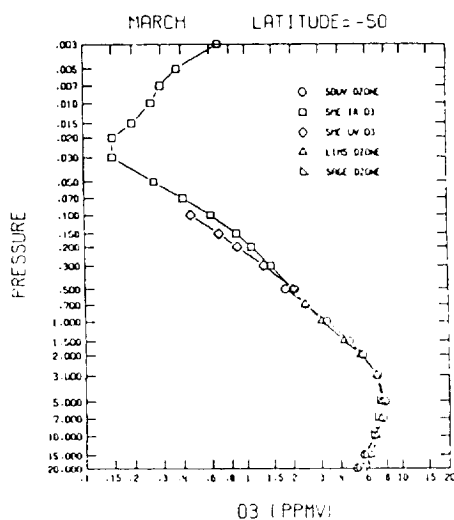


Figure 1. Comparison of ozone mixing ratios from five satellite experiments.

COMPARISON OF SAGE OZONE WITH REFERENCE MODEL (WORST CASE)  
(PERCENT DEVIATION FROM MODEL)

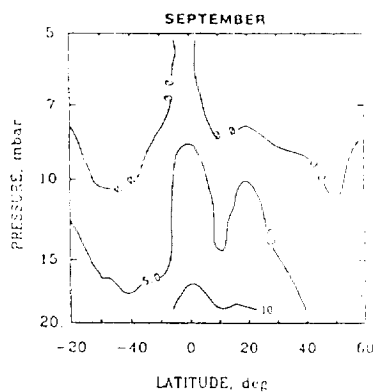


Figure 2. Comparison of reprocessed SAGE ozone data with improved reference model. The percent deviation from the model shown here represents the maximum deviations detected.

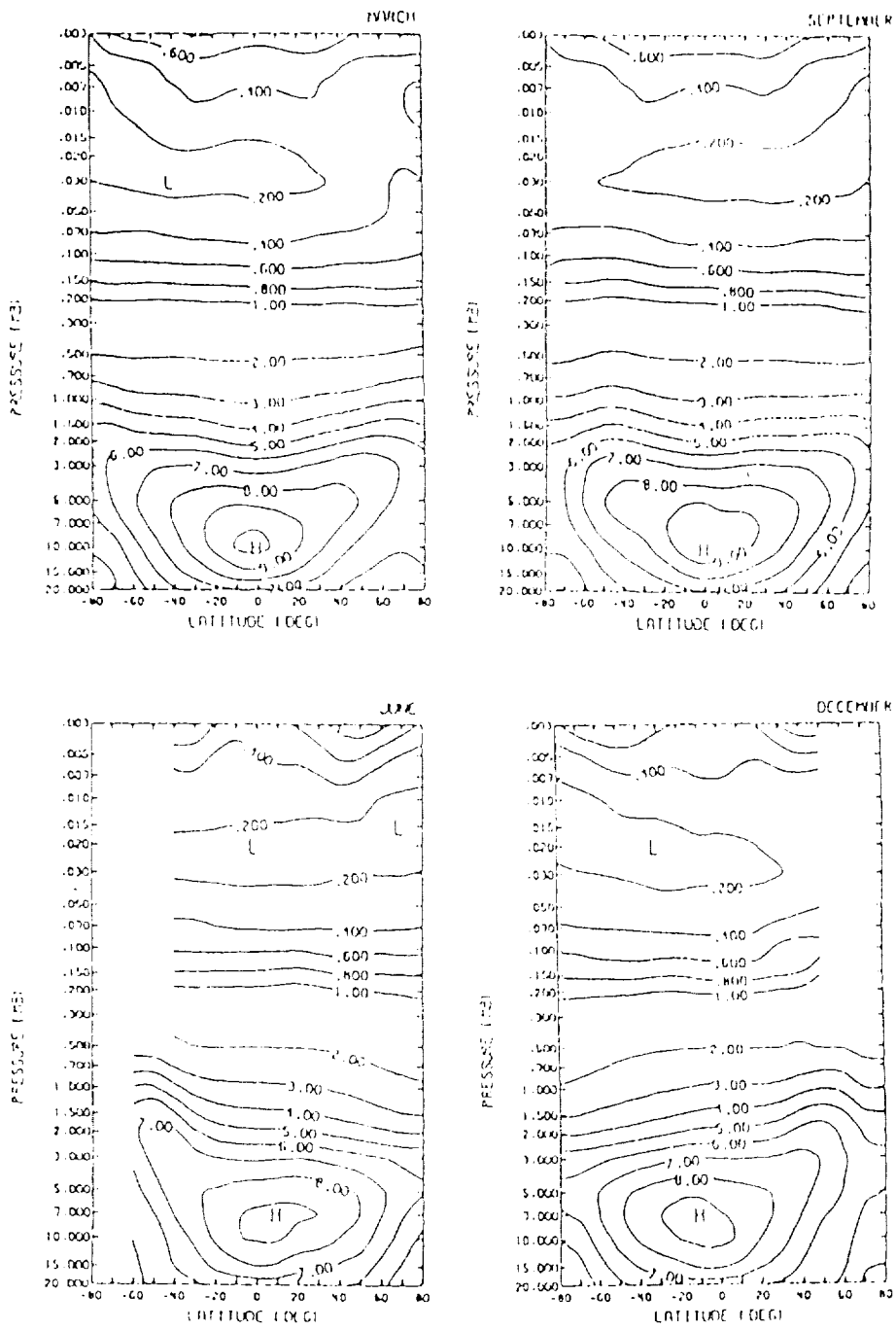


Figure 3. Improved reference model of ozone volume mixing ratios (ppmv).

COMPARISON BETWEEN KRUEGER-MINZNER MODEL  
AND SATELLITE MODEL OF OZONE

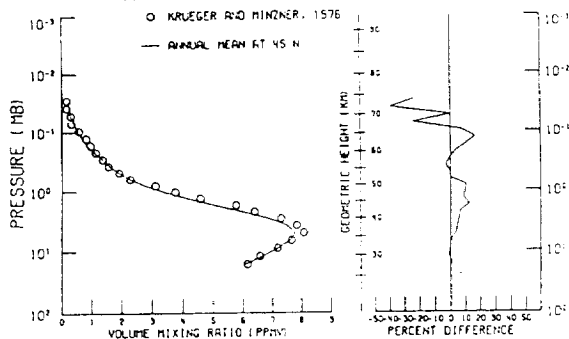
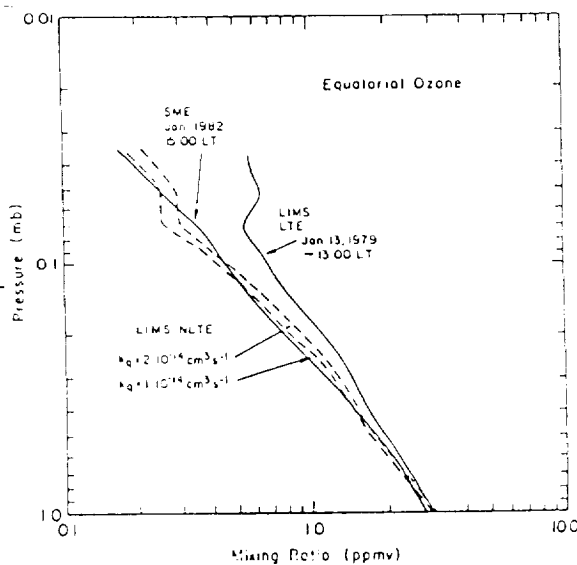


Figure 4. Comparison between Krueger-Minzner annual mean ozone model (45°N) and model of ozone based on satellite data.

Figure 5. Nimbus 7 LIMS measurements of dayside equatorial ozone (Jan. 13, 1979) before (LIMS LTE) and after (LIMS NLTE) correction for non-LTE effects. The two LIMS NLTE curves are for different quenching rates. Also shown is a comparison between SME dayside ozone measurements in January 1982 and the LIMS measurements corrected for non-LTE effects from (/16/).

DAYSIDE MESOSPHERIC OZONE MEASUREMENTS



NIGHT-DAY OZONE RATIO IN EQUATORIAL MESOSPHERE

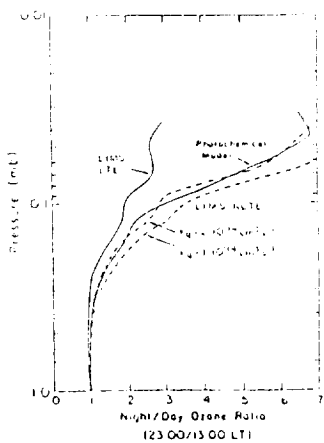


Figure 6. Night-to-day ozone ratio based on LIMS nightside measurements and the uncorrected (LIMS LTE) and corrected (LIMS NLTE) for the two quenching rates) LIMS dayside measurements. The observations are compared with the photochemical model of Garcia and Solomon /21/ (from /16/).

## COMPARISONS WITH SAGE

The Applications Explorer Mission-2 Stratospheric Aerosol and Gas Experiment (SAGE) used a four-channel Sun photometer which measured solar intensity at sunrise and sunset to derive ozone, aerosols, and  $\text{NO}_2$  concentrations. Absorption of 0.6 micron solar radiation by ozone allowed determination of the vertical structure of ozone to be obtained up to 30 times per day from February 1979 until November 1981. The early validation of the SAGE measurements is described in some detail by /6/ and /7/. Recently, the algorithm for determining ozone mixing ratios has been refined. We incorporate here a provisional version of the refined (sunset) data which has been provided by the experimenter. The data have been interpolated to the model latitudes, times, and pressures.

The reprocessed SAGE data is found to have very good agreement with the ozone reference model. Shown in Figure 1 is an example of the agreement between the five data sets used to generate the models of the ozone vertical structure from 20 mb to 0.003 mb ( $\approx$  25-90 km). Note that the mixing ratio is displayed on a log scale to allow accurate representation of the two orders of magnitude variation over this altitude range. It should be recognized that each data set represent entirely different techniques of measuring the vertical structure of ozone. The agreement shown is fairly representative. The reprocessed monthly SAGE data is shown by right triangles and closely matches the other data sets.

The vertical structure models are generated giving the 4-year mean of the SBUV data a weight of 2 due to the combination of extensive temporal and spacial coverage, while the other shorter data sets are given a weight of 1. The resulting updated model is compared with the reprocessed SAGE data in Figure 2. Over the latitudinal range of SAGE data provided for September, the SAGE data gives values near the Equator which are less than 15 percent higher than the reference model. This is the worst case of all months and results in less than a 4 percent modification in the reference model at 20 mb near the Equator for September. Thus, there are very small differences between this reference model, which is available upon request, and the Keating and Pitts tabulation /4/.

The resulting ozone distributions for the equinox and solstice months are shown in Figure 3. Shown in Figure 4 is a comparison of the Krueger and Minzner /8/ annual mean ozone reference model of 45N latitude, which is given in the U.S. Standard Atmosphere, 1976, and the updated ozone reference model provided here. The Krueger and Minzner model is based on rocket and balloon soundings and takes into account the latitudinal gradients in ozone near 45N from Nimbus 4 BUY observations. As may be seen, there is good agreement between the balloon and rocket model and the satellite measurement model, especially over the pressure range of the SAGE measurements incorporated here.

## NIGHTSIDE MESOSPHERIC MODEL

The SME mesospheric measurements from which the mesospheric ozone models are based are dayside measurements ( $\approx$  3 p.m.). Observations and theoretical models show that mesospheric ozone is higher on the nightside (Hilsenrath /9/; Anderson et al. /10/; Wilson and Schwartz /11/; Lean /12/; Vaughan /13/; Remsberg et al. /14/; Allen et al. /15/; Solomon et al. /16/; Green et al. /17/; Lobsiger and Kunzi /18/; Bjarnason et al. /19/). The Nimbus 7 Limb Infrared Monitor of the Stratosphere (LIMS) (Russell /20/) obtained mesospheric measurements on both the nightside and dayside. The LIMS instrument, a six-channel cryogenically cooled radiometer, had a number of channels to measure temperature and various species and included an ozone channel near 9.6 microns. Detailed validation studies have been described by Remsberg et al. /14/. Solomon et al. /16/ have shown that the LIMS dayside measurements of the mesosphere should be corrected for nonlocal thermodynamic equilibrium (non-LTE) effects. Shown in Figure 5 is an example of a LIMS dayside profile before (LIMS LTE) and after (LIMS NLTE) correction for non-LTE effects. After this correction, Solomon et al. /16/ point out there was good agreement between dayside LIMS and SME measurements. Shown in Figure 6 is the night-day ozone ratio based on LIMS nightside measurements and the uncorrected (LIMS LTE) and corrected (LIMS NLTE for two quenching rates) LIMS dayside measurements. As may be seen after the non-LTE correction, the ozone ratio is in good agreement with the photochemical model. The photochemical model results shown in the figure employ the photochemistry in the 2-dimensional model of Garcia and Solomon /21/. Since the correction for non-LTE effects in the dayside mesosphere have not been applied to the LIMS data as a whole, we have chosen to use only the SME data to represent the dayside mesosphere and nightside LIMS data to represent the nightside mesosphere.

Shown in Table 2 are the monthly nightside (ascending) zonal means of Kalman-filtered LIMS ozone volume mixing ratios (ppmv) (Remsberg et al. /22/) from the LIMS Map Archival Tape

TABLE 2 Nightside Mesospheric Ozone Volume Mixing Ratios (ppmv)

O3	ZONAL MEAN OCT															
	-60.	-50.	-40.	-30.	-20.	-10.	0.	10.	20.	30.	40.	50.	60.	70.	80.	
0.05	---	---	---	---	---	---	---	---	---	---	1.47	1.39	1.38	1.59	2.08	2.17
0.07	---	---	---	---	---	---	---	---	---	---	1.36	1.32	1.35	1.42	1.61	1.66
0.10	1.48	1.59	1.55	1.52	1.47	1.61	1.63	1.57	1.42	1.38	1.29	1.33	1.31	1.30	1.31	
0.15	1.46	1.48	1.45	1.44	1.41	1.46	1.46	1.43	1.38	1.31	1.28	1.29	1.26	1.22	1.21	
0.20	1.49	1.48	1.45	1.45	1.43	1.45	1.43	1.41	1.42	1.37	1.34	1.34	1.31	1.27	1.24	
0.30	1.58	1.55	1.53	1.54	1.54	1.56	1.53	1.53	1.55	1.51	1.49	1.47	1.45	1.45	1.43	
0.50	1.92	1.87	1.86	1.87	1.88	1.90	1.88	1.87	1.89	1.91	1.94	1.99	2.03	2.08	1.96	
O3	ZONAL MEAN NOV															
	-60.	-50.	-40.	-30.	-20.	-10.	0.	10.	20.	30.	40.	50.	60.	70.	80.	
0.05	---	---	---	---	---	---	---	---	---	---	1.51	1.40	1.39	1.68	2.20	2.14
0.07	---	---	---	---	---	---	---	---	---	---	1.42	1.33	1.31	1.49	1.68	1.73
0.10	---	1.63	1.60	1.56	1.48	1.50	1.46	1.49	1.44	1.37	1.30	1.27	1.29	1.33	1.43	
0.15	---	1.49	1.48	1.46	1.39	1.39	1.36	1.38	1.48	1.35	1.30	1.25	1.24	1.22	1.24	
0.20	---	1.47	1.46	1.46	1.41	1.39	1.36	1.39	1.43	1.48	1.36	1.31	1.29	1.24	1.22	
0.30	---	1.53	1.54	1.56	1.52	1.51	1.47	1.52	1.56	1.54	1.58	1.44	1.42	1.38	1.33	
0.50	---	1.83	1.84	1.87	1.87	1.89	1.86	1.89	1.92	1.94	1.99	2.01	2.03	1.95	1.85	
O3	ZONAL MEAN DEC															
	-60.	-50.	-40.	-30.	-20.	-10.	0.	10.	20.	30.	40.	50.	60.	70.	80.	
0.05	---	---	---	---	1.46	1.42	1.40*	---	1.50*	1.40*	1.54*	1.63	2.17	2.31	2.06	
0.07	---	---	---	---	1.43	1.36	1.33	---	1.38	1.40	1.42	1.47	1.70	1.78	1.72	
0.10	---	1.72	1.75	1.60	1.41	1.33	1.30	1.32	1.33	1.41	1.36	1.36	1.38	1.41	1.45	
0.15	---	1.55	1.55	1.48	1.37	1.31	1.27	1.30	1.35	1.41	1.36	1.31	1.27	1.26	1.27	
0.20	---	1.51	1.50	1.45	1.40	1.35	1.32	1.35	1.41	1.46	1.41	1.35	1.29	1.24	1.23	
0.30	---	1.56	1.56	1.54	1.51	1.48	1.45	1.49	1.54	1.57	1.52	1.46	1.41	1.38	1.26	
0.50	---	1.84	1.85	1.86	1.87	1.90	1.90	1.92	1.92	1.94	1.96	1.96	1.88	1.78	1.63	
O3	ZONAL MEAN JAN															
	-60.	-50.	-40.	-30.	-20.	-10.	0.	10.	20.	30.	40.	50.	60.	70.	80.	
0.05	---	---	---	---	1.41	1.43	1.47*	1.51*	1.49	1.48*	1.41*	1.72*	2.06*	2.32	2.28	
0.07	---	---	---	---	1.32	1.35	1.39	1.43	1.48	1.43	1.43	1.56	1.71	1.84	1.80	
0.10	---	1.73	1.73	1.46	1.29	1.31	1.34	1.37	1.35	1.40	1.45	1.46	1.47	1.49	1.47	
0.15	---	1.55	1.55	1.41	1.31	1.32	1.33	1.34	1.34	1.41	1.45	1.42	1.39	1.35	1.32	
0.20	---	1.52	1.51	1.45	1.38	1.37	1.37	1.39	1.47	1.52	1.47	1.42	1.34	1.31	1.31	
0.30	---	1.59	1.60	1.56	1.51	1.48	1.43	1.47	1.52	1.61	1.64	1.61	1.55	1.45	1.48	
0.50	---	1.89	1.92	1.92	1.89	1.83	1.78	1.84	1.91	2.01	2.11	2.11	2.05	1.88	1.78	
O3	ZONAL MEAN FEB															
	-60.	-50.	-40.	-30.	-20.	-10.	0.	10.	20.	30.	40.	50.	60.	70.	80.	
0.05	---	---	---	---	1.35*	1.50*	1.63	1.68*	1.58	1.44	1.50	1.60	2.01	2.52	2.65	
0.07	---	---	---	---	1.31	1.43	1.51	1.52	1.42	1.37	1.45	1.58	1.71	1.93	2.01	
0.10	1.12	1.69	1.58	1.34	1.30	1.48	1.44	1.46	1.38	1.35	1.42	1.44	1.51	1.53	1.58	
0.15	1.23	1.54	1.48	1.35	1.32	1.39	1.48	1.48	1.36	1.37	1.41	1.48	1.43	1.43	1.48	
0.20	1.34	1.52	1.49	1.41	1.39	1.43	1.42	1.42	1.48	1.45	1.46	1.46	1.47	1.47	1.51	
0.30	1.52	1.61	1.60	1.55	1.50	1.52	1.50	1.52	1.54	1.58	1.61	1.61	1.64	1.67	1.71	
0.50	1.90	1.94	1.98	1.97	1.89	1.86	1.82	1.86	1.91	2.01	2.09	2.16	2.25	2.27	2.21	
O3	ZONAL MEAN MAR															
	-60.	-50.	-40.	-30.	-20.	-10.	0.	10.	20.	30.	40.	50.	60.	70.	80.	
0.05	1.83	---	---	---	---	---	---	---	1.77*	1.57*	1.70	1.74	1.77	2.07	1.88	
0.07	1.59	---	---	---	---	---	---	---	1.62	1.49	1.57	1.64	1.70	1.88	1.62	
0.10	2.44	1.48	1.38	1.36	1.45	1.61	1.65	1.60	1.52	1.44	1.48	1.56	1.63	1.62	1.46	
0.15	1.42	1.45	1.38	1.37	1.43	1.52	1.53	1.48	1.45	1.41	1.44	1.47	1.51	1.51	1.44	
0.20	1.47	1.48	1.44	1.42	1.47	1.52	1.52	1.48	1.48	1.45	1.47	1.49	1.52	1.54	1.53	
0.30	1.59	1.59	1.56	1.54	1.57	1.61	1.59	1.58	1.59	1.59	1.59	1.61	1.63	1.67	1.76	
0.50	1.98	1.97	1.96	1.93	1.93	1.94	1.91	1.94	1.99	2.01	2.02	2.04	2.12	2.27	2.45	
O3	ZONAL MEAN APR															
	-60.	-50.	-40.	-30.	-20.	-10.	0.	10.	20.	30.	40.	50.	60.	70.	80.	
0.05	1.39	1.34	1.37*	1.58	---	---	---	---	---	---	1.78*	2.17	2.38	2.26	1.68	
0.07	1.34	1.29	1.27	1.37	---	---	---	---	---	---	1.68	1.88	2.02	1.99	1.58	
0.10	1.31	1.27	1.23	1.31	1.53	1.75	1.79	1.76	1.65	1.60	1.63	1.76	1.77	1.51	---	
0.15	1.27	1.28	1.28	1.35	1.48	1.60	1.62	1.59	1.55	1.52	1.53	1.59	1.59	1.44	---	
0.20	1.32	1.35	1.36	1.41	1.50	1.58	1.59	1.57	1.56	1.53	1.54	1.57	1.56	1.47	---	
0.30	1.48	1.51	1.50	1.53	1.60	1.65	1.66	1.66	1.65	1.65	1.65	1.65	1.65	1.61	---	
0.50	2.02	2.00	1.94	1.92	1.90	1.99	1.98	2.01	2.04	2.04	2.05	2.08	2.08	2.01	---	
O3	ZONAL MEAN MAY															
	-60.	-50.	-40.	-30.	-20.	-10.	0.	10.	20.	30.	40.	50.	60.	70.	80.	
0.05	1.84*	1.16*	1.18*	1.37*	---	---	---	---	---	---	---	---	---	---	---	
0.07	1.52	1.28	1.28	1.38	---	---	---	---	---	---	---	---	---	---	---	
0.10	1.31	1.25	1.23	1.27	1.46	1.68	1.74	1.72	1.65	1.72	1.85	1.94	1.86	---	---	
0.15	1.23	1.24	1.25	1.38	1.42	1.55	1.59	1.58	1.55	1.59	1.66	1.72	1.65	---	---	
0.20	1.28	1.32	1.33	1.37	1.45	1.54	1.57	1.56	1.56	1.59	1.63	1.67	1.68	---	---	
0.30	1.43	1.51	1.51	1.52	1.56	1.63	1.65	1.65	1.69	1.70	1.71	1.72	1.66	---	---	
0.50	2.11	2.13	2.04	1.95	1.94	1.95	1.96	1.99	2.05	2.06	2.05	2.03	1.96	---	---	

\* ESTIMATED ERROR EXCEEDS 20 PERCENT

(LAMAT) interpolated to the standard levels in the models. An "\*" is placed after values where the error in zonal mean is estimated to exceed 20 percent. Values are shown between 0.5 mb and 0.05 mb (when available) from 60S to 80N. Values between 50S and 60N are near 10 p.m. At the highest latitudes, earlier local solar times occur.

Shown in Figure 7 is the reference model for January, Equator. The LIMS nighttime values from 1 mb to 0.05 mb are seen to depart from the dayside model above 0.5 mb (= 54 km). Below 0.5 mb, little diurnal variability occurs due to the lower dayside O/O<sub>2</sub> ratio at lower altitudes resulting in less production of ozone on the nightside. In Figure 8, a similar pattern is shown for January, 60N (winter). Again, substantial day-night variations do not appear to occur below 0.5 mb. Referring to the table, it may be seen that a minimum mixing ratio generally occurs on the nightside near 0.2 mb (= 61 km). As may be seen in Figures 7 and 8, a dayside minimum occurs at much higher altitudes, 75 or 80 km.

Shown in Figure 9 is the night-day ozone ratio for January, based on 1980 LIMS (= 10 p.m.) and 1982-1983 SME (= 3 p.m.) data, as a function of latitude and pressure. It should be taken into consideration that as opposed to all of the difference being diurnal, part may be due to interannual variations and biases of SME data relative to LIMS data, even though the agreement between dayside SME and LIMS in Figure 9 appears to be in accord with the observed and predicted values given in Figure 6.

Figure 10 gives a detailed view of latitudinal-seasonal variations in the night-day ozone ratio at 0.1 mb (= 66 km). Ratios at this level can exceed a factor of 3 and maximize during solstice periods near 45 degree latitude in summer and near the Equator during equinox periods. This may largely result from the dayside ozone being more strongly photodissociated by the more directly incident summer Sun at mid latitudes and the equinoctial Sun at the Equator.

#### COMPARISON OF MODEL WITH OTHER MEASUREMENTS

It is of interest to compare the ozone vertical structure model, which is based on satellite measurements, with ozone measurements obtained by other techniques. In Figure 4, a comparison has already been shown with the Krueger and Minzer (1976) model based on balloon and rocket data. Shown in Figure 11 is a comparison with the satellite data model (47°N, annual mean) of the annual mean vertical distribution from ozonesonde data from Hohenpeissenberg (FRG) (48°N, 11°E) over the period 1967-1985 and from Thalwil-Payerne (Switzerland) (47°N, 7°E) over the period 1967-1982, and the annual mean vertical structure from Umkehr data from Arosa, Switzerland (47°N, 10°E), over the period 1955-1983. The three data sets were generously provided by R. D. Bojkov /23/. Considering that the ozonesonde and Umkehr data do not represent a zonal average, but do represent conditions over a period of many years, the agreement is very good.

Over the period April 1984 to April 1985, a microwave radiometer was operated at Bern, Switzerland (47°N, 7°E), measuring the thermal emission of the rotational ozone transition at 142.2 GHz to determine stratospheric and mesospheric ozone abundances in the range of 25 to 75 km. Monthly mean ozone partial pressures for Umkehr layers 6-10 were calculated from over 300 daytime profiles. Shown in Figure 12 (Lobsinger /24/) are the resulting ozone profiles obtained by the microwave measurements (solid line) compared with Umkehr measurements from Arosa (dashed line), 20-year monthly mean Arosa Umkehr (crosses), and the Keating and Young /1/ ozone reference model (open circles). The differences with the reference model may be partially due to local year-to-year phase shifts relative to the zonal mean variations. Note the excellent agreement in the annual variation at Umkehr levels 7 and 8 between the reference model and Arosa Umkehr (20 years) measurements.

A comparison with other information is also made between the annual mean of the microwave measurements in Figure 13. Residuals are shown relative to the microwave measurements (Lobsinger /24/). The solid line is the 20-year annual average of Arosa Umkehr measurements, the dash-dotted line the Krueger and Minzner /8/ model, and the dashed line the Keating and Young MAP model /1/. With the exception of Umkehr levels 5 (= 22 mb) and 14 (= 0.04 mb), the annual microwave measurements agree very closely with other information.

An ozone measurement campaign was conducted at Natal, Brazil (6°S, 35°W) in March-April 1985, resulting in seven profiles from ROCOZ-A ozonesondes (Barnes et al. /25/). Shown in Figure 14 is comparison of a mean of the ROCOZ-A ozone measurements with the MAP Interim Ozone Model /1/. The agreement is excellent, with the Natal measurements averaging 2 percent higher than the MAP model with a 3 percent standard deviation. The agreement between ozone data in the mid-1980's with a model based on satellite data in the late 1970's and early 1980's has interesting implications concerning the amplitude of long-term trends.

### DIURNAL VARIATION OF OZONE IN MESOSPHERE

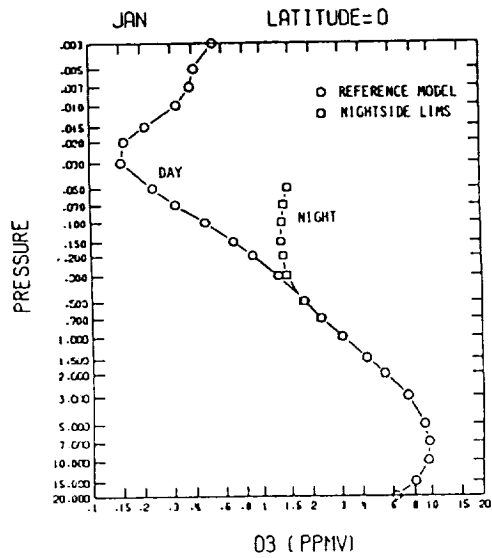


Figure 7. Diurnal variation of mesospheric ozone from satellite data. Comparison of ozone reference model (dayside above 0.5 mb) with the LIMS nightside measurements (0.05 mb to 1 mb) for Equator in January.

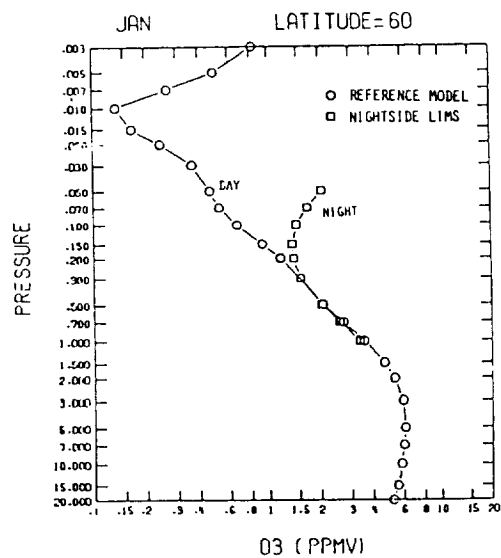


Figure 8. Same as Figure 7 but for 60°N in January.

NIGHT (LIMS) / DAY (SME) MESOSPHERIC OZONE RATIO

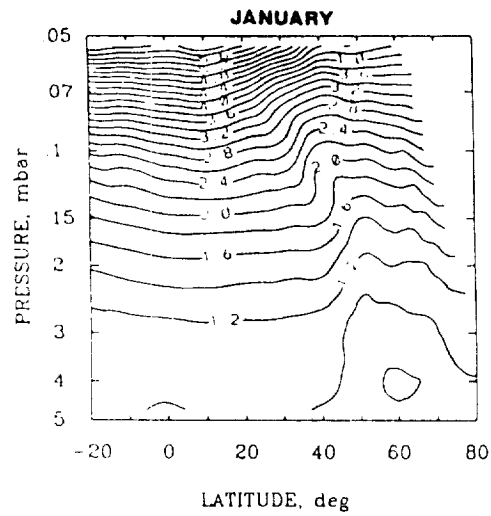


Figure 9. Night to day ozone ratio for January based on 1980 LIMS nightside data and 1982-1983 SME dayside data as a function of latitude and pressure.

NIGHT (LIMS) / DAY (SME) MESOSPHERIC OZONE RATIO

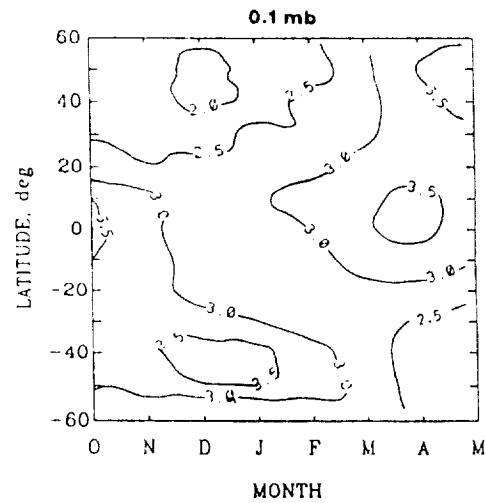


Figure 10. Night (LIMS) to day (SME) mesospheric ozone ratio at 0.1 mb ( $\approx$  66 km) as a function of latitude and season.

## OZONE REFERENCE MODEL AND LONG-TERM BALLOON AND UMKEHR MEASUREMENTS

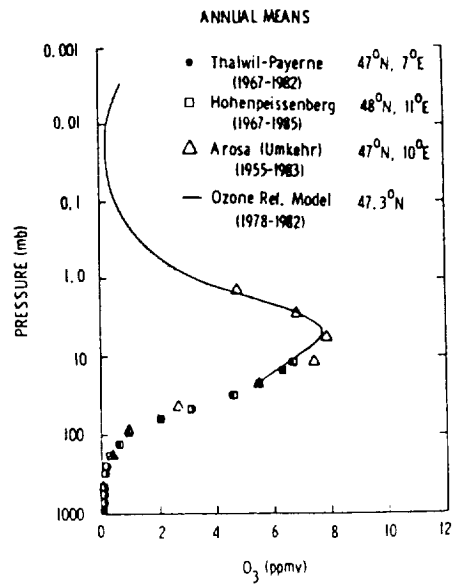


Figure 11. Comparison of ozone reference model based on satellite data with annual means of long-term balloon and Umkehr measurements.

## MONTHLY VARIATIONS IN OZONE NEAR 45N

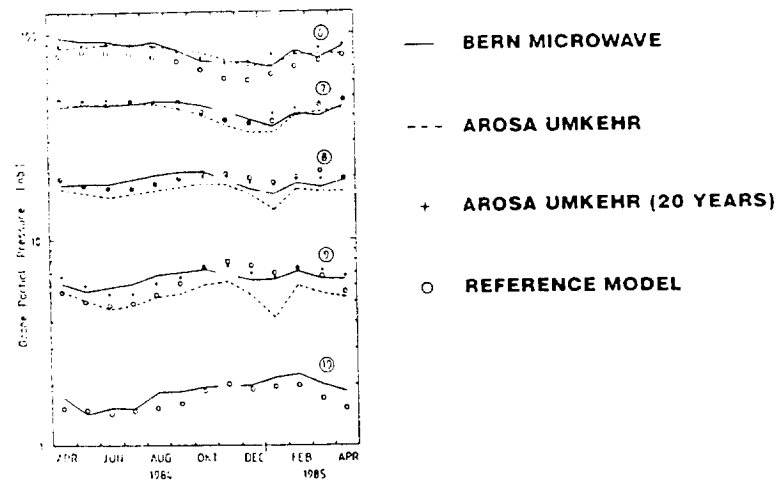


Figure 12. Comparison of monthly variations in ozone partial pressure from (a) microwave measurements from Bern, Switzerland, (b) simultaneous Umkehr measurements from Arosa, Switzerland, (c) 20 years of Umkehr measurements from Arosa, Switzerland, and (d) the ozone reference model based on satellite data (from /24/).

**RESIDUALS FROM ANNUAL MEAN OF MICROWAVE MEASUREMENTS  
(BERN)**

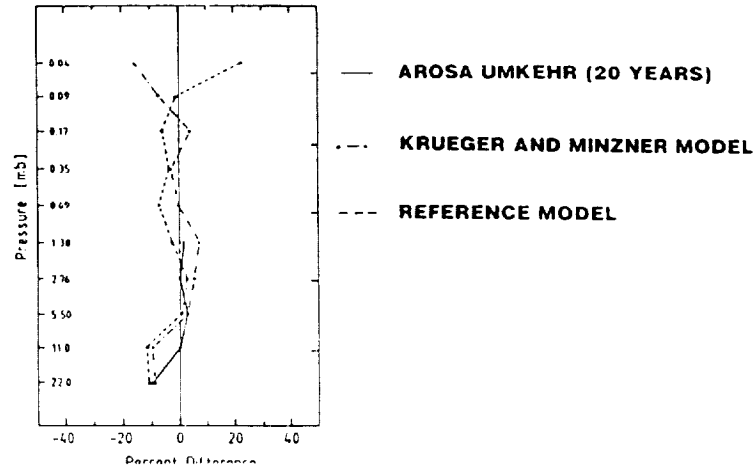


Figure 13. Residuals from annual mean of microwave ozone measurements from Bern, Switzerland of (a) 20 years of measurements from Arosa, Switzerland, (b) The Krueger and Minzner model /8/, and (c) the ozone reference model based on satellite data (from /24/).

**MEASUREMENTS OF EQUATORIAL OZONE**

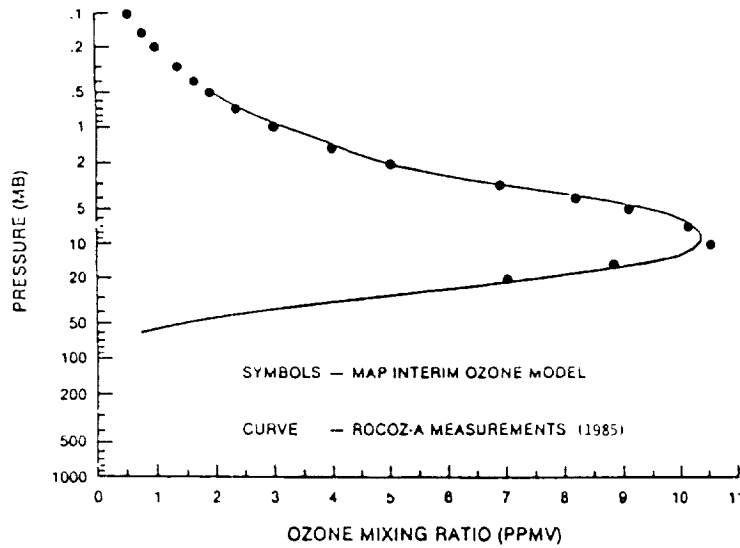


Figure 14. Comparison of equatorial ozone measurements obtained from 7 ROCOZ-A ozonesondes in 1985 with the ozone reference model based on satellite data (from /25/).

## REFERENCES

1. G.M. Keating and D.F. Young, Handbook of MAP, 16, 205 (1985)
2. G.M. Keating and D.F. Young, Adv. Space Res., 5, #7, 155 (1985)
3. G.M. Keating, D.F. Young, and M.C. Pitts, Adv. Space Res., 7, #10, 105 (1987)
4. G.M. Keating and M.C. Pitts, Adv. Space Res., 7, #9, 37 (1987)
5. C.L. Mateer, J.J. Deluisi, and C.C. Porco, NOAA TH ERL ARL-86, (1980)
6. M.P. McCormick, T.J. Swissler, E. Hilsenrath, A.J. Krueger, and M.T. Osborn, J. Geophys. Res., 89, 5315 (1984)
7. D.M. Cunnold, M.C. Pitts, and C.R. Trepte, J. Geophys. Res., 89, 5249 (1984)
8. A.J. Krueger and R.A. Minzner, J. Geophys. Res., 81, 4477 (1976)
9. E. Hilsenrath, J. Atmos. Sci., 28, 295 (1970)
10. G.P. Anderson, J.C. Gille, P.L. Bailey, and S. Solomon, paper presented at Quadriennial International Ozone Symposium, Int. Ozone Comm. and IAMAP, Boulder (1980)
11. W.J. Wilson and P.R. Schwartz, J. Geophys. Res., 86, 7385 (1981)
12. J.L. Lean, J. Geophys. Res., 87, 4973 (1982)
13. G. Vaughan, Nature, 296, 133 (1982)
14. E.E. Remsberg, J.M. Russell III, J.C. Gille, L.L. Gordley, P.L. Bailey, W.G. Planet, and J.E. Harries, J. Geophys. Res., 89, 5161 (1984)
15. M. Allen, J.I. Lunine, and Y.L. Yung, J. Geophys. Res., 89, 4841 (1984)
16. S. Solomon, J.T. Kiehl, B.J. Kerridge, E.E. Remsberg, and J.M. Russell III, J. Geophys. Res., 91, 9865 (1986)
17. B.D. Green, W.T. Rawlins, and R.M. Nadile, J. Geophys. Res., 91, 311 (1986)
18. E. Lobsinger and K.F. Kunzi, J. Atmos. Terr. Phys., 48, 1153 (1986)
19. G.G. Bjarnason, S. Solomon, and R.R. Garcia, J. Geophys. Res., 92, 5609 (1987)
20. J.M. Russell III, Adv. Space Res., 4, #4, 107 (1984)
21. R.R. Garcia and S. Solomon, J. Geophys. Res., 88, 1379 (1983)
22. E.E. Remsberg, R.J. Kurzeja, K.V. Haggard, J.M. Russell III, and L.L. Gordley, NASA Technical Report 2625 (1986)
23. R.O. Bojkov, private communication (1987)
24. E. Lobsinger, J. Atmos. Terr. Phys., 49, 493 (1987)
25. R.A. Barnes, A.C. Holland, and V.W.J.H. Kirchoff, J. Geophys. Res., 92, 5573 (1987)